Magnetic Cellulose Microcrystals with Tunable Magneto-Optical Responses

Xin Chen [a,b], Zuyang Ye [a], Fan Yang [a], Ji Feng [a], Zhiwei Li [a], Chen Huang [b], Qinfei Ke [b], Yadong Yin [a,*]

*Corresponding Author

E-mail: yadong.yin@ucr.edu

[a] *Department of Chemistry, University of California Riverside, Riverside, California 92521, United States*

[b] *Key Laboratory of Textile Science & Technology, Ministry of Education, College of Textiles, Donghua University, 2999 North Renmin Road, Songjiang, Shanghai 201620, P. R. China*

ABSTRACT

Magnetically actuated liquid crystals are potential alternatives to conventional liquid crystal systems in many applications thanks to their advantages of electrodeless operation, remote control, and low cost. However, their practical uses face a major challenge, namely the strong optical absorption of the magnetic components, which are mostly iron oxide-based materials. Here, we overcome this challenge by developing a nanocomposite composed of rod-shaped cellulose microcrystals with magnetite nanoparticles attached to their surfaces. This design takes advantage of the optical transparency and birefringence of the cellulose microcrystals, as well as their anisotropic shape which allows their efficient orientational alignment when their surfaces are modified by magnetite nanoparticles. Only a minimum amount of magnetite nanoparticles is required to enable instant and reversible orientational control of the cellulose microcrystals, ensuring a high degree of transparency of the system. These unique nanocomposites can be fixed in a polymer matrix with defined orientations at different regions by combining magnetic alignment and photolithography processes, producing thin films that appear near-transparent under the illumination of normal light and display patterns with high contrast when sandwiched between cross polarizers. This work reveals the enormous potential of the magnetic assembly strategy and making it a promising candidate for anti-counterfeiting applications.

Keywords: Magnetic; Cellulose microcrystals; Reversible tuning; Anisotropic optical property; Polarization.

1. Introduction

Liquid crystal materials have catalyzed many important applications in modern technology [1-3]. Combining liquid-like behavior and crystal-like ordering from molecular to macroscopic material levels, these self-assembled structures can be dynamically controlled by the application of external stimuli, such as electric and magnetic fields [4,5], or mechanical forces [6], leading to various functions, with a particularly successful example being the liquid crystal displays that are driven dominantly by electric fields [7,8]. For some applications, magnetically actuated liquid crystals with assembly behavior being manipulated by an external magnetic field have advantages such as remote control and low cost as their operation does not require transparent electrodes [9-12]. However, limited by toxicity and the required strength of the magnetic response, iron-based materials appear to be the only choices for most practical applications, although efforts have been made to the alignment of non-iron based nanostructures under extremely intense magnetic fields [13]. In the past few years, we and others have explored the direct use of ferro- and ferrimagnetic inorganic nanostructures to design magnetic liquid crystals, for example, by employing magnetic rod-like or disk-like iron oxide nanoparticles [14-18]. The drawback of these materials is that they all have strong absorption within the visible spectrum and typically display a dark brown color [19,20], which is usually undesirable in applications such as color display and anti-counterfeiting.

In this work, we propose to overcome the challenge by developing anisotropically shaped nanocomposites as the building blocks to construct magnetically responsive

liquid crystals. The key idea is to dope transparent nonmagnetic birefringent microcrystals with magnetic nanoparticles so that the loading of iron oxide in the system can be significantly minimized. Transparent cellulose microcrystals are chosen as the primary birefringent building blocks as they have rod-like shapes and their concentrated colloidal dispersion can exhibit liquid-like behavior and crystal-like ordering [21,22]. Moreover, they are the most abundant natural polymer produced in the biosphere and have many advantages in terms of sustainability, such as being renewable, nontoxic, cost-efficient, and easy to prepare [23,24]. We show that cellulose microcrystals can be conveniently made magnetically responsive through a simple coprecipitation method [25,26], which binds magnetic iron oxide nanoparticles with uniform distribution on their surfaces. Upon optimizing the loading amount of the iron oxide nanoparticles, the orientation of the resulting nanocomposites can be instantly and reversibly tuned using external magnetic fields while the dispersion remains near-transparent. The magnetic control further enables the fabrication of thin polymer films containing cellulose microcrystals with defined orientations in different regions. Such films are transparent under the illumination of normal light but display patterns with high contrast when observed under cross polarizers, making them promising candidates for anti-counterfeiting applications.

2. Materials and methods

2.1 Materials

Viscose fibers (cellulose fiber) were purchased from Sanyou Chemical Fiber, China.

Sulfuric acid (H_2SO_4) was purchased from Fisher Scientific, and ethyl alcohol (EG, denatured) and 2-hydroxy-2-methylpropiophenone (97%) from Sigma-Aldrich. Acrylamide (AM) and N, N′-Methylenebisacrylamide (BIS) were obtained from Fluka.

2.2 Synthesis of magnetic cellulose crystal

Hydrolysis of cellulose fibers. 2 g of cellulose fiber was mixed with 30 mL 40% (w/w) sulfuric acid at 65 °C. After 1 h acid hydrolysis reaction, the resultant suspension was diluted 20-fold with 600 mL of DI water and then stood still for 3 h to separate into layers. The lower suspension was centrifuged at 4000 rpm for 4 min, and then the precipitate was collected by removing the upper clear solution. This step was repeated five times by adding DI water until the pH of the final lower cellulose crystals suspension reached ≈7.0.

Synthesis of magnetic cellulose microcrystals. The above cellulose microcrystals suspension was mixed with 0.12 mmol $FeCl_3$, 0.24 mmol $FeCl_2$, and additional water to make a 50 mL solution, which was heated to 70 °C under nitrogen. Upon the addition of 0.96 mmol NaOH, the mixture was vigorously stirred for 30 min. The solution was then centrifuged at 2000 rpm and washed by DI water until no free Fe_3O_4 particles could be observed in the solution. The obtained precipitate was further cleaned by magnetic decantation using a permanent magnet. Finally, the resulting cellulose crystals were stored in a vacuum oven.

Fabrication of cellulose microcrystals/organogel film. A dispersion containing magnetic cellulose microcrystals (Φ = 0.15), acrylamide (AM, 250 mg), N,N'-Methylene-bis-acrylamide (BIS, 14 mg), 2-Hydroxy-2-methylpropiophenone (3μL),

and the solvent ethylene glycol (1 mL) was sandwiched between two glass slides. A photomask with a defined pattern was then placed on top of the sample, followed by the application of a magnetic field and UV exposure. Then the photomask was removed and the magnetic field was rotated by 45°, followed by another UV exposure.

2.3 Characterization

TEM images were taken on a Tecnai T12 transmission electron microscope operating at 120 kV. Optical diffraction spectra were measured on an Ocean Optics HR2000CG-UV-NIR spectrometer with a six-around-one reflection/backscattering probe.

3. Results and discussion

The cellulose microcrystals were extracted from cellulose fibers (Fig. S1) by hydrolysis in sulfuric acid (Fig. S2) [27,28]. After centrifugation, the resulting suspension was collected and dialyzed against Milli-Q water until reaching a neutral pH. As shown in Fig. 1a, the magnetic cellulose microcrystals were synthesized by coprecipitation of ferrous and ferric ions under an alkaline condition [29], producing Fe_3O_4 nanoparticles that were bound to the surface of cellulose microcrystals through the coordination between iron ions and hydroxyl groups. Free Fe_3O_4 nanoparticles were then separated and the magnetic cellulose microcrystals were collected by low-speed centrifugation (see the Supporting Information for the detailed process). The scanning electron microscopy (SEM) images in Fig. 1b(i), (i') demonstrated that there was no apparent morphological change in the cellulose microcrystals before and after doping with Fe_3O_4 nanoparticles. However, the transmission electron microscopy (TEM)

images in Fig. 1b(ii), (ii') clearly confirmed that Fe_3O_4 nanoparticles with an average overall diameter of ~10 nm (Fig. S3) were uniformly attached to the surface of cellulose microcrystals. The samples before and after coating were analyzed by X-ray diffraction (XRD) and Fourier Transform Infrared spectroscopy (FTIR). The cellulose fibers show no peaks in the XRD pattern, indicating that the structure is dominated by the amorphous region. After hydrolysis and acid wash, the amorphous region was removed. Three peaks at 12, 20, and 22 degrees were observed, indicating the crystalline nature of the remaining cellulose microcrystals. After loading Fe_3O_4, the XRD pattern showed almost no change, suggesting that the Fe_3O_4 nanoparticles were very small in sizes, and the crystallinity of the cellulose structures was not disrupted by hydrolysis (Fig. 1c, Fig. S4) [30,31].

Benefiting from the simplicity of the coprecipitation method and the low cost of the cellulose and iron oxide, the magnetic cellulose microcrystals can be conveniently produced in a large quantity, as demonstrated in Fig. 1d.

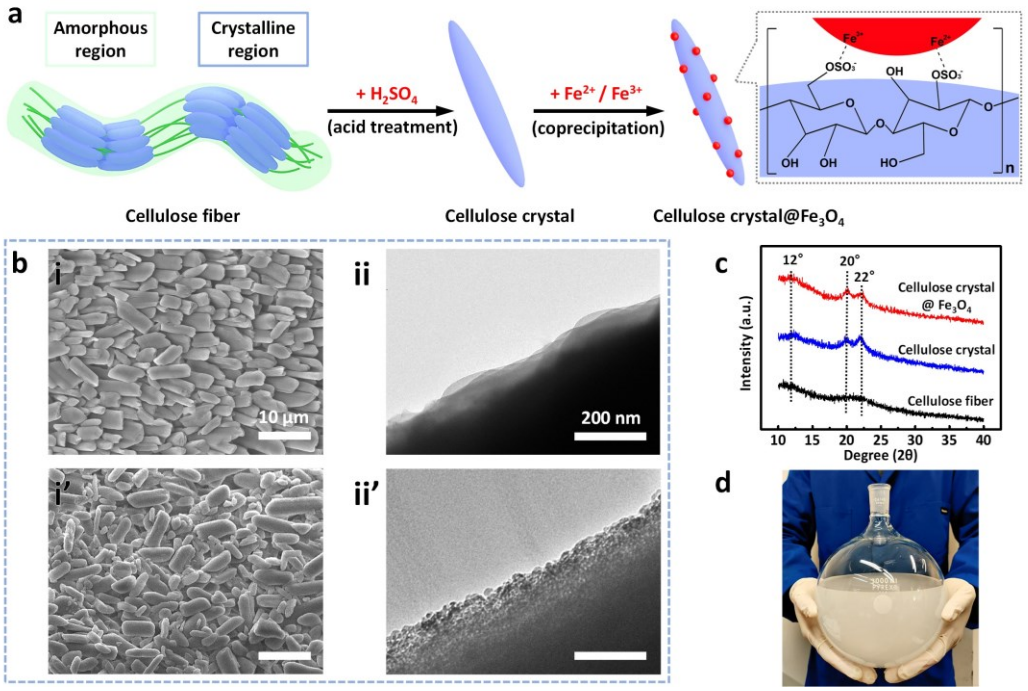

Fig. 1. (a) Schematic representation of the magnetic cellulose microcrystals synthesis. (b) SEM image of cellulose microcrystals (i) and magnetic cellulose microcrystals (i'). TEM images of the crystal surface before (ii) and after magnetization (ii'). (c) XRD of cellulose fibers, cellulose microcrystals, and cellulose microcrystals@Fe_3O_4. (d) Digital photo of a large production of magnetic cellulose microcrystals.

The loading amount of Fe_3O_4 nanoparticles on the cellulose microcrystals has to be optimized to balance the visible absorption and magnetic response. Fig. 2a provides the photographs of aqueous dispersions of the cellulose microcrystals containing 0, 2.32, 7.44, and 11.69 wt‰ Fe_3O_4 nanoparticles, all with a fixed volume fraction (Φ) of 1%. The amounts of Fe_3O_4 nanoparticles were determined by thermogravimetric analysis (Fig. S5). Increasing the amount of Fe_3O_4 nanoparticles on the cellulose microcrystals led to a darker color and stronger light absorption (Fig. 2b). On the other side, a higher loading of Fe_3O_4 nanoparticles enhances the magnetic response. As illustrated in Fig. 2c, the cellulose microcrystals without Fe_3O_4 nanoparticles were disorderly arranged,

while the magnetic cellulose microcrystals were aligned parallel to the direction of the external magnetic field. As expected, the alignment improved with the increase of the loading amount of the magnetic nanoparticles. Upon removal of the external magnetic field, the cellulose microcrystals returned to a random dispersion without aggregation, suggesting a superparamagnetic behavior. As shown in Fig. 2d, all of the samples display very small magnetic hysteresis loops, supporting their ferrimagnetic nature and paramagnetic responses. Further, the measurements of magnetic properties provided evidence that the saturated magnetization and the coercivity gradually increased with the loading amounts of the Fe_3O_4 nanoparticles. Given their effective magnetic response and low light absorption, the magnetic cellulose microcrystals with a loading amount of ~ 7.44 wt‰ were chosen for the subsequent studies.

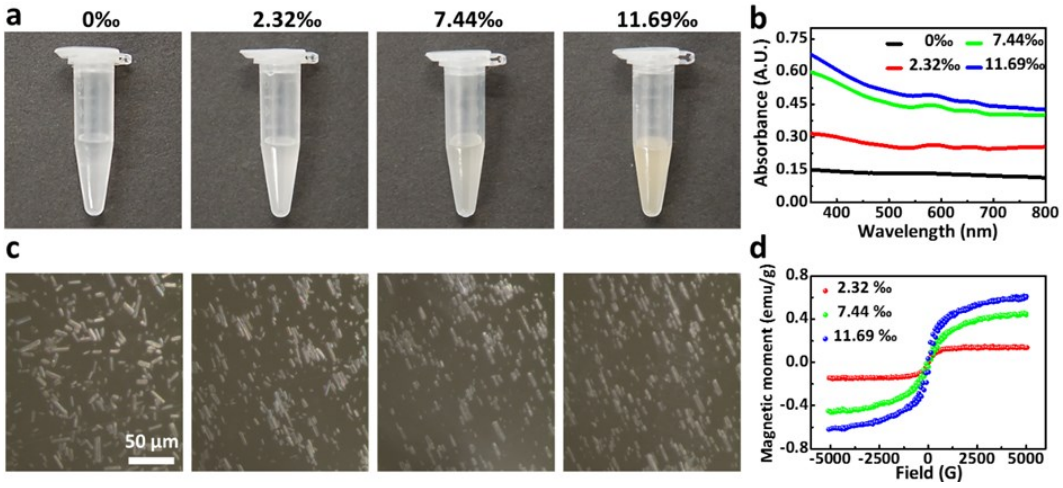

Fig. 2. (a) Digital images of cellulose microcrystals containing Fe_3O_4 nanoparticles of 0, 2.32, 7.44, and 11.69 wt‰. (b) Light absorption spectra of magnetic cellulose microcrystals suspension. (c) Optical microscopy (OM) images of aqueous dispersions of cellulose microcrystals and magnetic cellulose microcrystals showing the arrangement under the external magnetic field. (d) The magnetic hysteresis loop of magnetic cellulose microcrystals with various Fe_3O_4 nanoparticles content.

Fig. 3a schematically illustrates the optical switching property of magnetic cellulose microcrystals in response to the changes in the direction of the magnetic field (B). The intensity of light transmission through magnetic cellulose microcrystals sandwiched between cross polarizers can be described as:

$$I = I_0 \sin^2(2\alpha) \sin^2(\pi \Delta n L/\lambda)$$

where I_0 is the intensity of light passing through the first polarizer; α is the angle between the transmission axes of the polarizer and the long axis of the liquid crystal; Δn is the difference in the refractive indices along the long axis and short axis for liquid crystals aligned at a specific angle; L is the sample thickness; λ is the wavelength of the incident light [32]. Obviously, the intensity would reach the maximum as α changes to 45°. The polarized optical microscopy (POM) images (Fig. 3b) and Video S1 provided more visualized evidence. By rotating the magnetic field, one could control the orientation of the cellulose microcrystals in a dispersion sandwiched between cross polarizers to achieve continuous optical switching. Bright views appeared when the magnetic cellulose microcrystals are aligned along the field direction of 45° against the polarizer, while nearly no light intensity was observed when the field direction was parallel or perpendicular to the polarizers. In contrast, the same sample did not show apparent change when observed under the bright field mode (with parallel polarizers) in Fig. 3c.

The volume fraction (Φ) of the magnetic cellulose microcrystals in the liquid film is an important factor that affects the total transmittance and the bright/dark contrast [33].

As shown in Fig. 3d, increasing the volume fraction of magnetic cellulose microcrystals reduced the transmittance but enhanced the contrast (which is defined here by the intensity of light (λ=600 nm) transmitted through a liquid crystal sandwiched between cross polarizers as the magnetic field turns to 45° relative to the polarizer). The suspensions with Φ ranging from 0.1 to 0.2 could not only have over 60% in transmittance but also exhibit a sufficiently high contrast that was clearly observable. The magnetic cellulose microcrystals exhibited a reasonably rapid response to the changes in the magnetic field direction. As shown in Fig. 3e, a 30-μL suspension (Φ=0.1) sandwiched between cross polarizers could respond to a magnetic field with switching frequencies of 1.27 Hz (red), 2.12 Hz (green) and 3.18 Hz (blue), while no transmittance change was observed in a control sample without magnetic cellulose microcrystals (black curve).

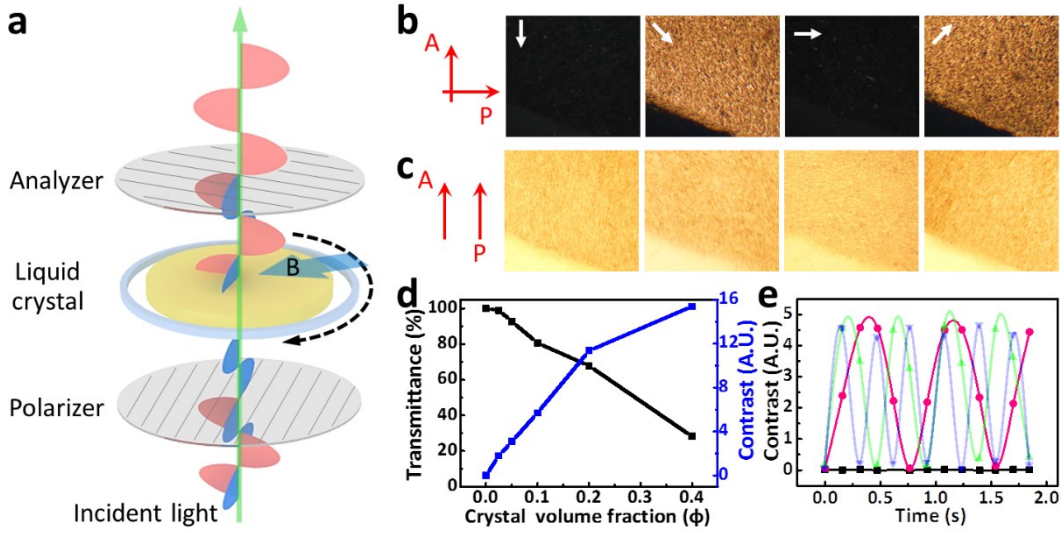

Fig. 3. (a) Schematic illustration of the magnetically-actuated optical switching process. (b, c) POM images (b) and bright-field optical microscopy images (c) of magnetic liquid crystals in the solution under magnetic fields oriented in different directions. Red

arrows indicate the transmission axis of the polarizer (P) and analyzer (A), and white ones indicate the magnetic field direction. The bottom-left corner in each image contains no sample. (d) The transmittance and contrast of cellulose@Fe_3O_4 with different volume fractions. (e) The transmittance profile of a magnetic liquid crystal under a variable-frequency rotating magnetic field.

A unique feature of magnetic cellulose microcrystals is that their orientation in a dispersion can be conveniently controlled by an external magnetic field and then fixed by solidifying the dispersing media. Such a property can be combined with photolithographic techniques to create patterns with optical anisotropy for designing novel security devices, as schematically illustrated in Fig. 4a. Specifically, we first sandwiched a dispersion containing magnetic cellulose microcrystals (Φ = 0.15), monomer (AM), crosslinker (BIS), photoinitiator, and solvent ethylene glycol between two glass slides. A photomask with a defined pattern was then placed on top of the sample, followed by the application of a magnetic field (B1). Upon exposure to UV light, the orientation of the magnetic cellulose microcrystals in the uncovered regions was fixed along B1 direction within the plane. In the second step, the photomask was removed and the magnetic field was then rotated by 45° (B2). Another exposure of the sample to UV light led to the formation of a thin polymer film containing patterns of different optical polarization [34,35].

As expected, the transparency of the film depends on the volume fraction of the magnetic cellulose microcrystals (Fig. S6). Thanks to the low concentration of iron oxide nanoparticles, the transmittance of the films could remain ~ 80% at the volume fraction of 0.1 and ~ 60% at 0.2. As shown in Fig. 4b, for a film with a volume fraction

of 0.15, no pattern can be noticed by the naked eye when viewed under normal light. However, as demonstrated in Fig. 4c, a clear contrast was observed when it is placed under a polarized optical microscope (POM). This optical anisotropy is due to the different orientations of the cellulose microcrystals with respect to the transmission axis of the polarizer: the parallel case appeared as dark (region II), and the one with 45° tilt appeared as bright (region I), which is consistent with Equation 1. The orientation of the microcrystal is further revealed by increasing the magnification of the microscope, as shown in Fig. 4d and Fig. 4e. To fabricate films with macroscopic patterns, we used a photomask of 4.5 cm × 4 cm shown in Fig. 4f. After UV exposure, the film exhibited no apparent contrast between the two regions (Fig. 4g). When the thin film was placed between the cross polarizers, shifting the transmission axis of the polarizer to be parallel to the direction of regions II reversed the dark and bright areas (Fig. 4h and Fig. 4i).

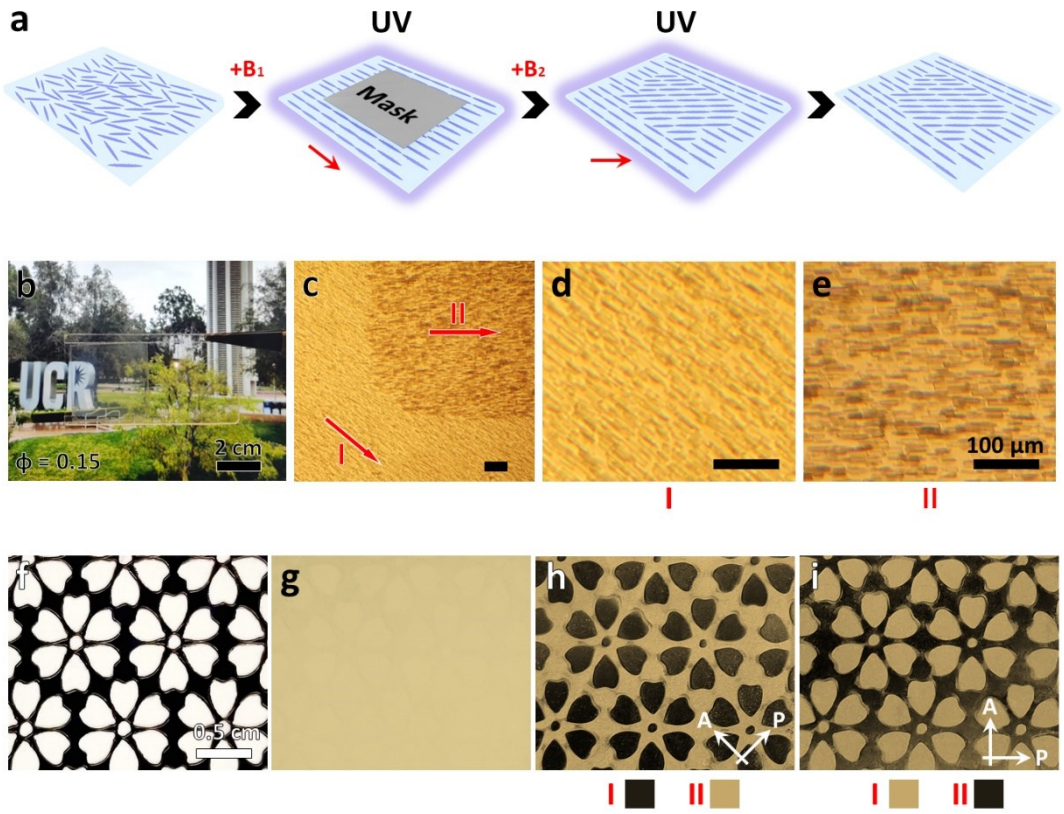

Fig. 4. (a) Scheme showing the lithography process for patterning a polymer film that contains magnetic cellulose microcrystals with different orientations in different regions. (b) Digital image showing the transparency of the patterned film (Φ = 0.15) under normal light. (c) POM images of the two regions with magnetic cellulose microcrystals aligned at 45° (I) and 0° (II) with respect to the transmission axis of the polarizer (which is set to be horizontal). (d, e) Magnified POM images show the orientations of the microcrystals in the region I and region II. (f) Mask for printing a flower pattern in the polymer film. (g) Digital image of the film under normal light. (h, i) Digital images of the film sandwiched between cross polarizers before (h) and after (i) shifting the direction of the transmission axis of the polarizers for 45°. All the scale bars in images (c-e) represent 100 μm, and images (f-i) are in the same scale.

4. Conclusions

In conclusion, we have developed magnetically responsive liquid crystals by integrating the magnetic properties of magnetite nanoparticles with the rod-shape and birefringent property of cellulose microcrystals. The unique design allows us to reduce

the absorption of the system and produce near-transparent films, and therefore addresses a major challenge in previous magnetically responsive liquid crystal systems where highly absorptive pure iron oxide nanostructures were used as the primary building blocks. The rod shape of the cellulose microcrystals and the surface modification with magnetite nanoparticles enable their efficient alignment by external magnetic fields, making it convenient to dynamically control the light transmittance when their colloidal dispersion is sandwiched between the cross polarizers. By combining magnetic alignment and photolithography, we can further fabricate thin polymer films that appear transparent under the illumination of normal light but display patterns with high contrast when sandwiched between cross polarizers. Our new magnetically responsive liquid crystals feature several advantages, including instant and reversible tunability, near-transparency, low cost and high abundance of the materials, and easy incorporation into polymer films and convenient patterning, making them attractive for many practical applications ranging from optical switches to information displays, and anti-counterfeiting devices.

Acknowledgements

We are grateful for the financial support from the U.S. National Science Foundation (DMR-1810485) and the Fundamental Research Funds for the Central Universities (18D310124).

Supplementary data

Supplementary data associated with this article can be found in the online version.

References

[1] I. H. Lin, D. S. Miller, P. J. Bertics, C. J. Murphy, J. J. de Pablo, N. L. Abbott, Endotoxin-induced structural transformations in liquid crystalline droplets, Science 32 (2011) 1297-1300. http://doi.org/10.1126/science.1195639.

[2] Z. Q. Pei, Y. Yang, Q. M. Chen, E. M. Terentjev, Y. Wei, Y. Ji, Mouldable liquid-crystalline elastomer actuators with exchangeable covalent bonds, Nat. Mater. 13 (2014) 36-41. http://doi.org/ 10.1038/nmat3812.

[3] H. K. Bisoyi, S. Kumar, Liquid-crystal nanoscience: an emerging avenue of soft self-assembly, Chem. Soc. Rev. 40 (2011) 306-319. http://doi.org/10.1039/b901793n.

[4] H. K. Bisoyi, T. J. Bunning, Q. Li, Stimuli-driven control of the helical axis of self-organized soft helical superstructures, Adv. Mater. 30 (2018) 1706512. http://doi.org/10.1002/adma.201706512.

[5] J. H. Kim, M. Yoneya, H. Yokoyama, Tristable nematic liquid-crystal device using micropatterned surface alignment, Nature 420 (2002) 156-162. http://doi.org/10.1038/nature01163.

[6] K. Ariga, T. Mori, J. P. Hill, Mechanical control of nanomaterials and nanosystems, Adv. Mater. 24 (2012) 158-176. http://doi.org/10.1002/adma.201102617.

[7] L. Wang, Q. Li, Stimuli-directing self-organized 3D liquid-crystalline nanostructures: from materials design to photonic applications, Adv. Funct. Mater. 26 (2016) 10-28. http://doi.org/10.1002/adfm.201502071.

[8] Z. G. Zheng, Y. N. Li, H. K. Bisoyi, L. Wang, T. J. Bunning, Q. Li, Three-dimensional control of the helical axis of a chiral nematic liquid crystal by light, Nature 531 (2016) 352-356. http://doi.org/10.1038/nature17141.

[9] L. B. Hu, H. S. Kim, J. Y. Lee, P. Peumans, Y. Cui, Scalable coating and properties of transparent, flexible, silver nanowire electrodes, ACS Nano 4 (2010) 2955-2963. http://doi.org/10.1021/nn1005232.

[10] H. A. Becerril, J. Mao, Z. Liu, R. M. Stoltenberg, Z. N. Bao, Y. S. Chen, Evaluation of solution-processed reduced graphene oxide films as transparent conductors, ACS Nano 2 (2008) 463-470. http://doi.org/10.1021/nn700375n

[11] S. Bae, H. Kim, Y. Lee, X. F. Xu, J. S. Park, Y. Zheng, J. Balakrishnan, T. Lei, R. H. Kim, Y. I. Song, Y. J. Kim, K. S. Kim, B. Ozyilmaz, J. H. Ahn, B. H. Hong, S. Iijima, Roll-to-roll production of 30-inch graphene films for transparent electrodes, Nat. Nanotechnol. 5 (2010) 574-578. http://doi.org/10.1038/nnano.2010.132.

[12] A. Kim, Y. Won, K. Woo, S. Jeong, J. Moon, All-solution-processed indium-free transparent composite electrodes based on Ag nanowire and metal oxide for thin-film solar cells, Adv. Funct. Mater. 24 (2014) 2462-2471. http://doi.org/10.1002/adfm.201303518.

[13] M. Nakayama, S. Kajiyama, A. Kumamoto, T. Nishimura, Y. Ikuhara, M. Yamato, T. Kato, Stimuli-responsive hydroxyapatite liquid crystal with macroscopically controllable ordering and magneto-optical functions, Nat. Commun. 9 (2018) 568. http://doi.org/10.1038/s41467-018-02932-7.

[14] S. Umadevi, X. Feng, T. Hegmann, Large area self-assembly of nematic liquid-crystal-functionalized gold nanorods, Adv. Funct. Mater. 23 (2013) 1393-1403. http://doi.org/10.1002/adfm.201202727.

[15] M. S. Wang, L. He, S. Zorba, Y. D. Yin, Magnetically actuated liquid crystals, Nano Lett. 14 (2014) 3966-3971. http://doi.org/10.1021/nl501302s.

[16]S. W. Zhang, W. Q. Xu, M. Y. Zeng, J. Li, J. X. Li, J. Z. Xu, X. K. Wang, Superior adsorption capacity of hierarchical iron oxide@magnesium silicate magnetic nanorods for fast removal of organic pollutants from aqueous solution, J. Mater. Chem. A 1 (2013) 11691. http://doi.org/10.1039/c3ta12767b.

[17]B. Klöckner, P. Daniel, M. Brehmer, W. Tremel, R. Zentel, Liquid crystalline phases from polymer functionalized ferri-magnetic Fe_3O_4 nanorods, J. Mater. Chem. C 5 (2017) 6688-6696. http://doi.org/10.1039/c7tc01106g.

[18]M. Shuai, A. Klittnick, Y. Shen, G. P. Smith, M. R. Tuchband, C. Zhu, R. G. Petschek, A. Mertelj, D. Lisjak, M. Copic, J. E. Maclennan, M. A. Glaser, N. A. Clark, Spontaneous liquid crystal and ferromagnetic ordering of colloidal magnetic nanoplates, Nat. Commun. 7 (2016) 10394. http://doi.org/10.1038/ncomms10394.

[19]D. Y. Li, Y. G. Zhang, Y. L. Zhang, X. F. Zhou, S. J. Guo, Fabrication of bidirectionally doped β-Bi_2O_3/TiO_2-NTs with enhanced photocatalysis under visible light irradiation, J. Hazard. Mater. 258 (2013) 42-49. http://doi.org/10.1016/j.jhazmat.2013.02.058.

[20]S. C. Alfaro, S. Lafon, J. L. Rajot, P. Formenti, A. Gaudichet, M. Maille´, Iron oxides and light absorption by pure desert dust: An experimental study, J. Geophys. Res. 109 (2004) D08208. http://doi.org/10.1029/2003JD004374.

[21]S. N. Fernandes, P. L. Almeida, N. Monge, L. E. Aguirre, D. Reis, C. L. P. de Oliveira, A. M. F. Neto, P. Pieranski, M. H. Godinho, Mind the microgap in iridescent cellulose nanocrystal films, Adv. Mater. 29 (2017) 1603560. http://doi.org/10.1002/adma.201603560.

[22]H. Q. Huang, X. J. Wang, J. C. Yu, Y. Chen, H. Ji, Y. M. Zhang, F. Rehfeldt, Y. Wang, K. Zhang, Liquid-behaviors-assisted fabrication of multidimensional birefringent materials from

dynamic hybrid hydrogels, ACS Nano 13 (2019) 3867-3874. http://doi.org/10.1021/acsnano.9b00551.

[23]R. J. Moon, A. Martini, J. Nairn, J. Simonsen, J. Youngblood, Cellulose nanomaterials review: structure, properties and nanocomposites, Chem. Soc. Rev. 40 (2011) 3941-3994. http://doi.org/ 10.1039/c0cs00108b.

[24]M. Giese, L. K. Blusch, M. K. Khan, M. J. MacLachlan, Functional materials from cellulose-derived liquid-crystal templates, Angew. Chem. Int. Ed. 54 (2015) 2888-2910. http://doi.org/10.1002/anie.201407141.

[25]J. Q. Guo, I. Filpponen, L. S. Johansson, P. Mohammadi, M. Latikka, M. B. Linder, R. H. A. Ras, O. J. Rojas, Complexes of magnetic nanoparticles with cellulose nanocrystals as regenerable, highly efficient, and selective platform for protein separation, Biomacromolecules 18 (2017) 898-905. http://doi.org/10.1021/acs.biomac.6b01778.

[26]L. Peng, P. F. Qin, M. Lei, Q. R Zeng, H. J. Song, J. Yang, J. H. Shao, B. H. Liao, J. D. Gu, Modifying Fe_3O_4 nanoparticles with humic acid for removal of Rhodamine B in water, J. Hazard. Mater. 209 (2012) 193-198. http://doi.org/10.1016/j.jhazmat.2012.01.011.

[27]K. Yao, Q. J. Meng, V. Bulone, Q. Zhou, Flexible and responsive chiral nematic cellulose nanocrystal/poly(ethylene glycol) composite films with uniform and tunable structural color, Adv. Mater. 29 (2017) 1701323. http://doi.org/10.1002/adma.201701323.

[28]H. L. Zhu, W. Luo, P. N. Ciesielski, Z. Q. Fang, J. Y. Zhu, G. Henriksson, M. E. Himmel, L. B. Hu, Wood-derived materials for green electronics, biological devices, and energy applications, Chem. Rev. 116 (2016) 9305-9374. http://doi.org/10.1021/acs.chemrev.6b00225.

[29]K. Z. Liu, L. Han, P. F. Tang, K. M. Yang, D. L. Gan, X.Wang, K. F. Wang, F. Z. Ren, L. M.

Fan, Y. G. Xu, Z. F. Lu, X. Lu, An anisotropic hydrogel based on mussel-inspired conductive ferrofluid composed of electromagnetic nanohybrids, Nano Lett. 19 (2019) 8343-8356. http://doi.org/10.1021/acs.nanolett.9b00363.

[30]H. B. Zhao, J. H. Kwak, Z. C. Zhang, H. M. Brown, B. W. Arey, J. E. Holladay, Studying cellulose fiber structure by SEM, XRD, NMR and acid hydrolysis, Carbohyd. Polym. 68 (2007) 235-241. http://doi.org/10.1016/j.carbpol.2006.12.013.

[31]K. Kulasinski, R. Guyer, D. Derome, J. Carmeliet, Water adsorption in wood microfibril-hemicellulose system: role of the crystalline−amorphous interface, Biomacromolecules 16 (2015) 2972-2978. http://doi.org/10.1021/acs.biomac.5b00878.

[32]M. J. Stephen, J. P. Straley, Physics of liquid crystals, Rev. Mod. Phys. 46 (1974) 617-704.

[33]T. Naganuma, Y. Kagawa, Effect of particle size on light transmittance of glass particle dispersed epoxy matrix optical composites, Acta Mater. 47 (1999) 4321-4327. http://doi.org/10.1016/S1359-6454(99)00329-8.

[34]J. Feng, F. Yang, X. J. Wang, F. L. Lyu, Z. W. Li, Y. D. Yin, Self-aligned anisotropic plasmonic nanostructures, Adv. Mater. 31 (2019) 1900789. http://doi.org/10.1002/adma.201900789.

[35]Z. W. Li, M. S. Wang, X. L. Zhang, D. W. Wang, W. J. Xu, Y. D. Yin, Magnetic assembly of nanocubes for orientation-dependent photonic responses, Nano Lett. 19 (2019) 6673-6680. http://doi.org/10.1021/acs.nanolett.9b02984.